FABRY-PEROT INTERFEROMETER BASED IMAGING OF ATMOSPHERIC TRACE GASES

Jonas Kuhn[1], Ulrich Platt[2], Nicole Bobrowski[3], Peter Lübcke[4] and Thomas Wagner[5]

1. Institute of Environmental Physics, Heidelberg University, Heidelberg, Germany; Max Planck Institute for Chemistry, Mainz, Germany; jonas.kuhn@iup.uni-heidelberg.de
2. Institute of Environmental Physics, Heidelberg University, Heidelberg, Germany; Max Planck Institute for Chemistry, Mainz, Germany; ulrich.platt@iup.uni-heidelberg.de
3. Institute of Environmental Physics, Heidelberg University, Heidelberg, Germany; Max Planck Institute for Chemistry, Mainz, Germany; Nicole.bobrowski@iup.uni-heidelberg.de
4. Institute of Environmental Physics, Heidelberg University, Heidelberg, Germany; peter.luebcke@iup.uni-heidelberg.de
5. Max Planck Institute for Chemistry, Mainz, Germany; thomas.wagner@mpic.de

ABSTRACT

Standard techniques (e.g. Differential Optical Absorption Spectroscopy, DOAS) for trace gas remote sensing in the UV/VIS spectral range use dispersive spectroscopy to identify and quantify trace gases in the atmosphere using specific narrowband absorption structures of the molecular species. These methods have the advantage of high spectral resolution and thus, a high sensitivity and selectivity to many species. However, the technique is typically limited to a single viewing direction and limited by the light throughput of the spectrometer. While 2D imaging is possible by spatial scanning, the temporal resolution remains poor (several minutes per image). The intrinsic time scales of many processes involving, e.g. transport, turbulent mixing and chemistry at lower atmospheric altitudes, are often much shorter (order of seconds, e.g. point sources). Therefore, many processes cannot be directly resolved by dispersive methods.

We investigate the application of Fabry-Perot Interferometers (FPIs) for the optical remote sensing of atmospheric trace gases. By choosing a FPI transmission spectrum, which is optimised to correlate with narrowband (ideally periodic) absorption structures of the target trace gas in the UV/VIS, column densities of the trace gas can be determined with a high sensitivity and selectivity using only a few (carefully selected) spectral channels. Different from dispersive optical elements, the FPI can be implemented in 2D-full frame imaging setups (cameras) with high light throughput.

A prototype one pixel FPI instrument was designed for sulphur dioxide (SO_2) in the UV. Good agreement with conventional measurement techniques and high sensitivity is demonstrated and an extension to 2D-detection of SO_2 distributions should be straightforward. Calculations for the application of the FPI technique to other trace gases are introduced. We show that typical volcanic bromine monoxide (BrO) column densities (~$1*10^{14}$ molec cm^{-2}) could be quantified with an FPI camera with a time resolution of approximately one frame (20x20 pixels) per second.

KEYWORDS IMAGING, FABRY PEROT INTERFEROMETER, SULPHUR DIOXIDE, BROMINE MONOXIDE, VOLCANOES

INTRODUCTION

Within the last decades, progress in optical remote sensing of atmospheric trace gases led to a better understanding of many important processes including air pollution, stratospheric ozone destruction, halogen chemistry, and the evolution of volcanic plumes. Narrowband structures in the trace gas molecule's absorption spectrum are used to quantify the amount of gas within a line of

DOI:

sight, i.e. its column density (CD, typically in units of molec cm^{-2}) and to separate its signal from interfering gas species and scattering processes.

Differential Optical Absorption Spectroscopy (DOAS, see (1) for details) has become a standard technique for atmospheric trace gas remote sensing in the UV/VIS with high sensitivity (detection limits within the ppb to ppt range). A dispersive spectrometer and a telescope with a narrow field of view are used to record spectra I(λ) of scattered sunlight, which are compared to a Fraunhofer reference spectrum (FRS) $I_0(\lambda)$. Beer Lambert's law describes the respective spectral optical density τ(λ) with $\sigma_i(\lambda)$ and $c_i(l)$ describing the absorption cross section and the concentration of trace gas species i along a line of sight L:

$$\tau(\lambda) = -\log\frac{I(\lambda)}{I_0(\lambda)} = \int_0^L \sum_i \sigma_i(\lambda) c_i(l) dl + scattering\ at\ air\ molecules\ and\ aerosol$$

Atmospheric UV/Vis optical densities mostly consist of trace gas absorption and scattering processes at air molecules or aerosols. In order to exclude signatures of scattering, the spectral optical density τ(λ) can be high pass filtered. The narrowband contributions of the trace gases' absorption cross sections, known from the literature, are then fitted to the remaining narrowband optical density. Assuming the FRS does not contain the trace gas of interest the fit coefficients represent the CDs $S_i = \int_0^L c_i(l)\ dl$, i.e. the integral of the trace gas concentration along the light path of I(λ)

In principle, spatial distributions of trace gases (images or height profiles) can be recorded by whiskbroom (pixel by pixel) scanning or scanning of several elevation angles with a narrow FOV telescope (e.g. Multi-Axis DOAS, (2,3)). More complex optical setups allow to record spectra of an entire image column at once by using a two dimensional detector array (e.g. Imaging DOAS, (4)). Images can then be recorded by pushbroom (column by column) scanning.

However, the acquisition times of these techniques are rather high (several minutes per image or profile for typ. trace gas CDs) limiting their application to processes that are spatially homogeneous on that time scale.

Determination of two dimensional (2D) atmospheric trace gas distributions with high time resolution at time scales of the order of one second, i.e. fast imaging of atmospheric trace gases is possible with techniques recording all pixels of an image at once for different spectral channels. This allows studying phenomena which are not accessible to the conventional scanning methods, e.g. (see also (5)) :

1) Direct and quantitative visualization of atmospheric transport and turbulent mixing processes at their intrinsic time scales (of the order of seconds at lower altitudes).
2) Chemical transformation of spatial reactive trace gas gradients (e.g. the formation of halogen oxides) in real time e.g. BrO in volcanic plumes
3) The investigation of spatial reactive trace gas gradients (e.g. BrO) and their evolution

With fast trace gas imaging techniques sources and sinks of trace gases can be identified and quantified on much smaller spatial and temporal scales than with conventional remote sensing techniques. This allows for instance to gain insight into small scale mixing processes or to distinguish chemical conversions from transport.

Fast imaging techniques rely on non-dispersive wavelength selective elements in order to resolve spectral absorption features of trace gases. Most of the present atmospheric trace gas imaging schemes use a set of band pass filters (e.g. SO_2 Camera, see e.g. (6)) or a tuneable band pass filter as wavelength selective element (e.g. NO_2 Camera, (7)). This either involves intricate optical set-ups or yields a low spectral resolution and therefore high cross interferences.

We study the application of Fabry-Perot Interferometers (FPIs) as wavelength selective elements for trace gas imaging in the UV/VIS. The FPI transmission spectrum, which is approximately periodic in wavelength, is matched to the spectral absorption structures of trace gases that often show a similar

periodicity. Due to the high correlation of wavelength selective element and trace gas absorption spectrum a high sensitivitiy can be reached and cross interferences of other absorbers are minimized by only using a small number of spectral channels (see (8)). Air spaced FPI etalons are very robust devices and allow for simple optical designs with high spectral resolutions.

We present a proof of concept study of the technique for volcanic sulphur dioxide and validate the expected high accuracy and sensitivity of the technique. In a model study we adapt the measurement to BrO and show that the sensitivity and selectivity are high enough to image volcanic BrO CD distributions with one frame of 20x20 pixels per second, which is about 100 times faster than Imaging DOAS approaches.

METHODS

Validation of the FPI remote sensing technique - One Pixel FPI SO_2 device

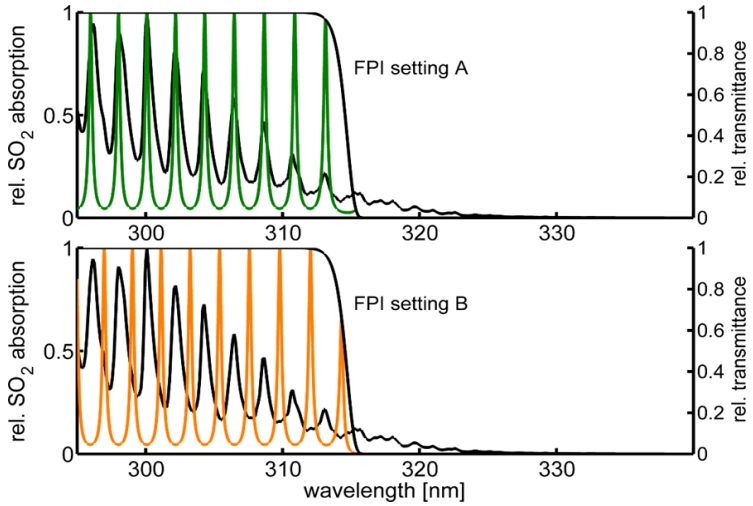

Figure 1: Two FPI settings (on/off absorption band) used in the One Pixel FPI SO_2 measurement

The measurement technique was validated with an FPI matched to the vibrational structure of SO_2 absorption in the UV. We used an air spaced etalon from SLS Optics Ltd. with a free spectral range of ~2.1nm and a finesse of ~7 across a clear aperture of 20mm. The spacer material of the air gap (Corning ULE glass) ensures a high temperature stability of the transmission profile (less than 1e-4 of a free spectral range for a 40K temperature change).

The optical setup of the prototype consists of a fused silica lens (f=50mm), which projects light from a narrow field of view (~0.8° opening angle) onto a photodiode. The FPI, which was mounted on a servo motor for tilt tuning and the band pass filter (~300nm – ~313nm) were placed in front of the lens.

The radiances for two FPI settings (on/off SO_2 absorption line, setting A/B in Figure 1) were recorded and evaluated according to Formula 1 (see below).

The SO_2 FPI device was co-aligned with a MAX DOAS instrument, which is a standard method for remote sensing of SO_2 in the atmosphere. An elevation motor was used to perform spatial scans.

Model study for BrO application

In principle, the FPI remote sensing technique can be applied to any molecule species with structured (ideally periodic) spectral absorption within the wavelength range of scattered sunlight. We examine the application to volcanic BrO in a model study. Volcanic BrO is present in much lower concentrations than volcanic SO_2 (BrO/SO_2 typ. 10^{-4}, see e.g. (9)). However, the BrO differential absorption cross section is by a factor of ~50 larger in a wavelength range with about one order of magnitude higher solar radiance (10).

The differential absorption optical density caused by typical volcanic BrO CDs is thereby by two orders of magnitudes weaker than that of SO_2. In addition, there are several other molecule species

absorbing with comparable differential optical densities across the wavelength window of BrO absorption (see Fig. 2).

The main focus of this model study is the determination of the BrO sensitivity and the evaluation of the impact of potentially cross interfering molecule species.

In order to model the instrument response of the measurement setup, the light intensities I_k reaching the detector of the instrument (e.g. CCD detector) were calculated:

$$I_k = \int d\lambda\, I_o(\lambda)\, e^{-\sum_i \sigma_i(\lambda) S_i}\, T_{BPF}\, T_{FPI}^k(\lambda)$$

$I_0(\lambda)$ is the spectrum of the incident scattered sunlight. A spectrum recorded in Heidelberg at a solar zenith angle of 73° (viewing direction: 160° azimuth relative to the sun, 1° elevation angle) was used for our calculations. S_i is the CD of an absorber i with absorption cross section $\sigma_i(\lambda)$. The absorption is added to the spectrum according to Beer Lambert's law. $T_{FPI}^k(\lambda)$ is the FPI transmittance in configuration k and $T_{BPF}(\lambda)$ the transmission of the bandpass filter preselecting the measurement wavelength range. For negligible absorption at the FPI's reflective surfaces, $T_{FPI}(\lambda)$ can be calculated with the so called Airy Formula:

$$T_{FPI}^k(\lambda) = \left[1 + C_F(R) \sin^2 \frac{\delta(\lambda; d, n, \alpha)}{2}\right]^{-1}$$

with $\delta(\lambda; d, n, \alpha) = \frac{2\pi}{\lambda} 2nd \cos\alpha$ and $C_F(R) = \frac{4R}{(1-R)^2}$

R is the reflectance of the FPI surfaces, d the separation of the surfaces, n the refractive index of the medium in between the surfaces and α the incidence angle of the incident light (plane wave).

$T_{BPF}(\lambda)$ was modelled with a higher-order Gaussian function:

$$T_{BPF}(\lambda; A, \mu, c, p) = A\, e^{-\left(\frac{(\mu-\lambda)^2}{2c^2}\right)^p}$$

with a full width at half maximum of

$$FWHM(c, p) = 2\sqrt{2} \log 2^{\frac{1}{2p}}.$$

A describes the peak transmission at the central wavelength μ. An order of p=4 was used to approximate realistic filter transmission profiles.

The instrument response of an FPI measurement can be described by the difference of the optical density τ_i measured with two FPI settings i=A, B:

$$R = \tau_A - \tau_B = -\log \frac{I_{A,M}}{I_{A,0}} + \log \frac{I_{B,M}}{I_{B,0}} \qquad (1)$$

The subscripts indicate measurement viewing direction (M, with 'plume absorption') and reference viewing direction (0, background, without 'plume absorption').

The absolute radiances for the photon budget calculations were inferred by scaling I_0 with a known absolute radiance according to (10).

Here the FPI method is investigated for volcanic BrO detection in the wavelength range at around 340nm. In this wavelength range several other gases (see Table 1) show structured absorption. Their absorptions were considered in typical high amounts in our spectral radiances in order to study the cross interferences of the individual gases.

We assume, that in the field of view of the imaging device we always have background intensity measurements included (i.e. the absorber plume does not cover the full field of view). This means that by being able to effectively correct for background variations, the FPI imaging technique is only sensitive to the difference of plume to background optical density.

Table 1: Gas species included into the model, typical high CDs were assumed in order to quantify potential cross interferences

Species	typ. high CD [molec cm^{-2}]	origin
BrO (11)	1*10^{14} molec cm^{-2}	volcanic
SO_2 (12)	3*10^{18} molec cm^{-2}	volcanic
OClO (13)	5*10^{13} molec cm^{-2}	volcanic
NO_2 (14)	1*10^{16} molec cm^{-2}	tropospheric background, pollution
HCHO (15)	5*10^{15} molec cm^{-2}	tropospheric background, pollution
O_3 (16)	3*10^{17} molec cm^{-2}	tropospheric background, pollution
O_4 (17)	1*10^{43} molec^2 cm^{-4}	O_2 collision

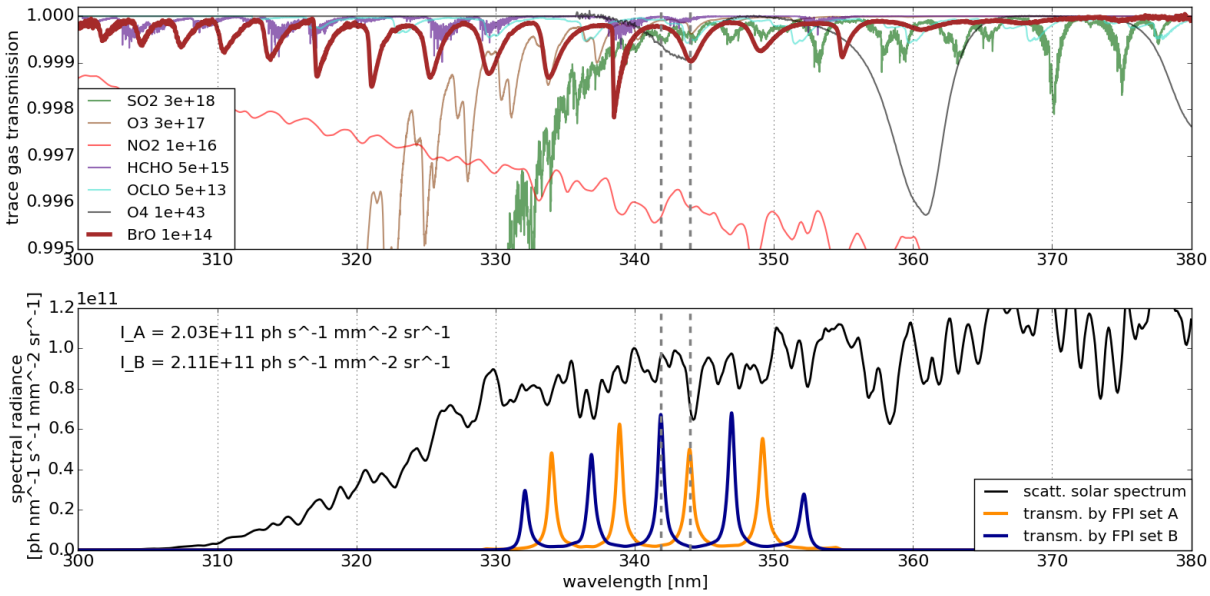

Figure 2: transmittance of typical amounts of trace gases at a volcano (upper panel); spectral radiance through two FPI settings matched to the BrO absorption cross section.

Imaging optical setup and photon budget

One method to implement the FPI technique in an imaging device is to parallelize the incident radiation from the image field of view before traversing the FPI. This is realized by an optics that is telecentric on the image side (see Figure 3). In order to avoid strong blurring of the FPI transmission spectrum, the divergence of the light beams traversing the FPI should not be larger than Θ=1° (corresponds to a spectral shift of ~1 FWHM for the FPI in our configuration which is tilted by ~5°). With a lens of focal length f this condition limits the maximum aperture radius to

$$a = f \tan\frac{\theta}{2}.$$

The FPI clear aperture radius a_{FPI} determines the camera field of view opening angle of

$$\gamma_{FOV} = 2 \arctan\frac{a_{FPI}}{f}.$$

The etendue per pixel is then determined by the spatial resolution of the recorded image, which can be varied by (hardware or software) binning. For n_{pix} being the number of pixels along a column of a square detector array, the etendue per pixel of the instrument is:

$$E_{pix} = A_{pix}\,\Omega_{pix} = a^2 \sin^2\left(\frac{\gamma_{FOV}}{2n_{pix}}\right)\pi^2 \qquad [sr\ mm^2]$$

The detectors quantum efficiency and losses within the optics are combined in an additional loss factor η. Each FPI channel (on-band and off-band setting) requires one image acquisition. We assume a photon electron shot noise limited measurement, i.e. $\Delta I/I \sim N_{ph}^{-1/2}$. The uncertainty in the instrument response R is then:

$$\Delta R_{pix} = \sqrt{2}\,\frac{\Delta I}{I} = \sqrt{\frac{2}{N_{ph,pix}}} \qquad \text{with} \qquad N_{ph,pix} = I E_{pix} \eta$$

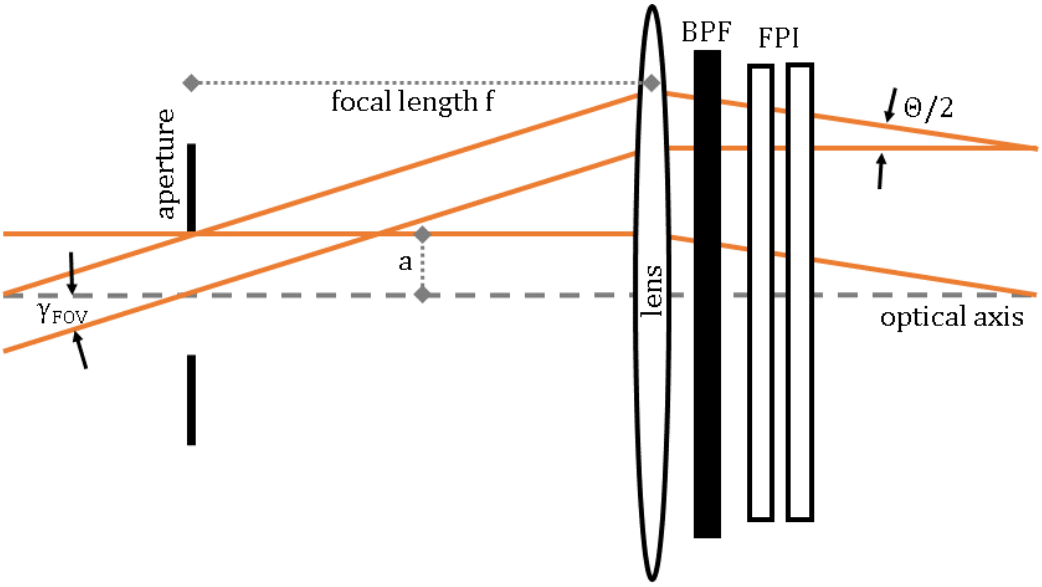

Figure 3: FPI camera optics (telecentric on the image side): incident radiation is parallelized before traversing the FPI and the band pass filter. The aperture determines the beam divergence, which determines the spectral resolution of the FPI and the light throughput of the instrument.

RESULTS

Proof of concept – One Pixel FPI SO_2 measurement at Mt. Etna volcano

Figure 4 shows the results of cross section scans of part of the plume of Mt. Etna volcano, Italy, performed with the FPI SO_2 instrument and the co-aligned DOAS spectrometer. Despite a not yet optimized FPI instrument design (limited accuracy of the servo motor used for tilt tuning the FPI, slight misalignment of the telescope's FOVs), the recorded time series shows good correlation with the DOAS time series. A high SO_2 sensitivity of the FPI technique is observed. Moreover, the FPI measurement shows a high stability towards the changing elevation angle. Typically, this introduces variations in aerosol extinction and ozone absorption, which are automatically corrected by the DOAS algorithm.

The introduced one pixel camera can be extended to a full frame camera. Either the light from the image field of view is parallelized before traversing the FPI (see Fig. 3) or the trace gas CDs can be retrieved from evolving ring structures across the camera FOV (see (8) for details). Cross interferences of presently used SO_2 Cameras, using two band pass filters (see. e.g. 6), would be drastically reduced.

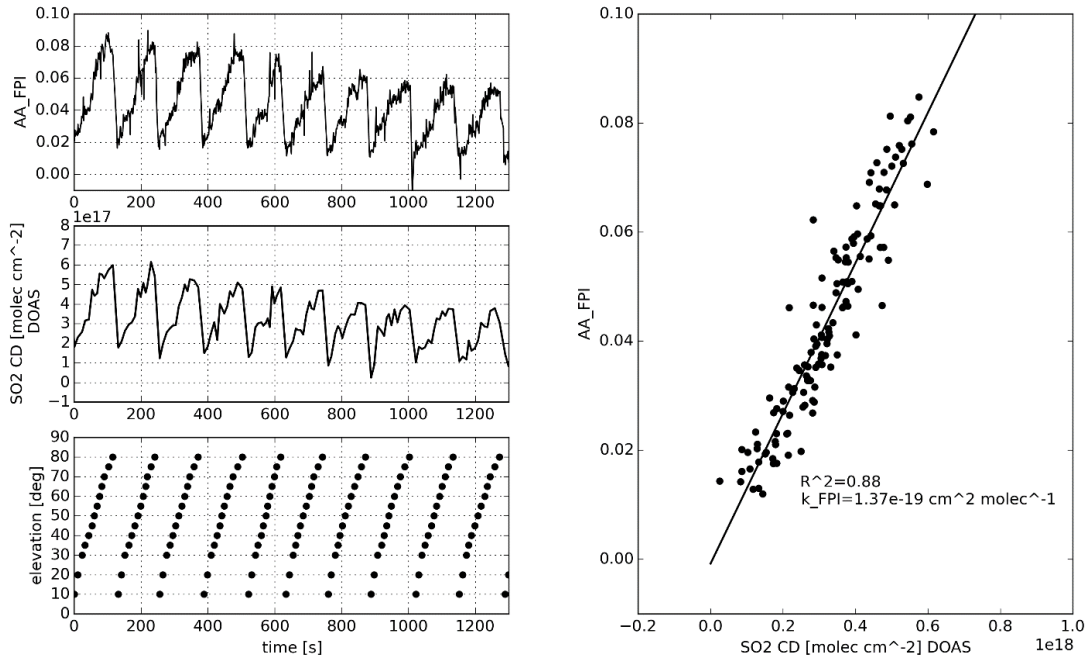

*Figure 4: Cross section scans of Mt. Etna's Plume. Left panel: Time series of the instrument response of the FPI SO_2 device (top), SO_2 CD measured with co-aligned MAX DOAS instrument (center), and elevation angle of the setup (bottom). Right panel: DOAS and FPI method show good correlation and a high sensitivity (~1.4*10^{-19} cm^2 molec^{-1}) was reached.*

Measurement wavelength range and FPI configuration for BrO

A band pass filter is used to isolate the measurement wavelength range. Within the wavelength range, there should be strong periodical absorption structures of the target gas to which the FPI transmission is matched. Moreover, a low correlation of the other species absorption spectrum with the FPI transmission is required in order to minimize cross interferences.

For the following calculations an interference band pass filter with 342nm central wavelength and a FWHM of 20nm was assumed. The choice is a trade-off between BrO sensitivity (slightly stronger absorption bands at shorter wavelengths) and minimising ozone cross interference (correlation of spectral absorption of ozone and BrO towards shorter wavelengths). Such filters are commercially available and can be additionally tuned by tilting.

Figure 5 shows the differential optical density of BrO and the individual potentially interfering species within the preselected wavelength range for a varying FPI air gap d (FPI interferograms). The BrO optical density variation clearly dominates. Other molecule species also cause considerable variations in the optical density. However, they hardly correlate with the BrO signal and therefore an optimal FPI setting can be found that minimises their impact on the on-band/off-band measurement.

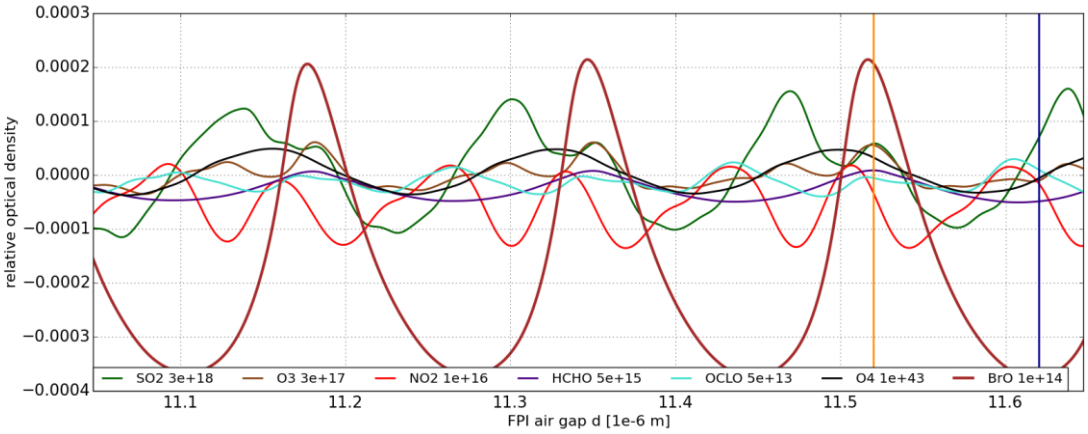

Figure 5: differential optical density of the different trace gases for varying FPI air gap within the measurement wavelength range (see Fig. 2). The FPI settings have to be chosen to maximize the BrO signal and at the same time minimise cross interferences.

Sensitivity and cross interferences of the FPI BrO measurement

Figure 6 shows the simulated calibration curve for the FPI settings indicated in Figure 5 (vertical lines). The influence of the interfering gases is indicated by the dashed lines, which illustrate the shift of the calibration curve caused by the influence of a typical high amount of the respective molecule species. With only two spectral channels the cross interferences are already very low, causing an uncertainty of ~3*10^{13} BrO molec cm^{-2} in the signal. By using more than two FPI settings the cross interferences can even be further reduced.

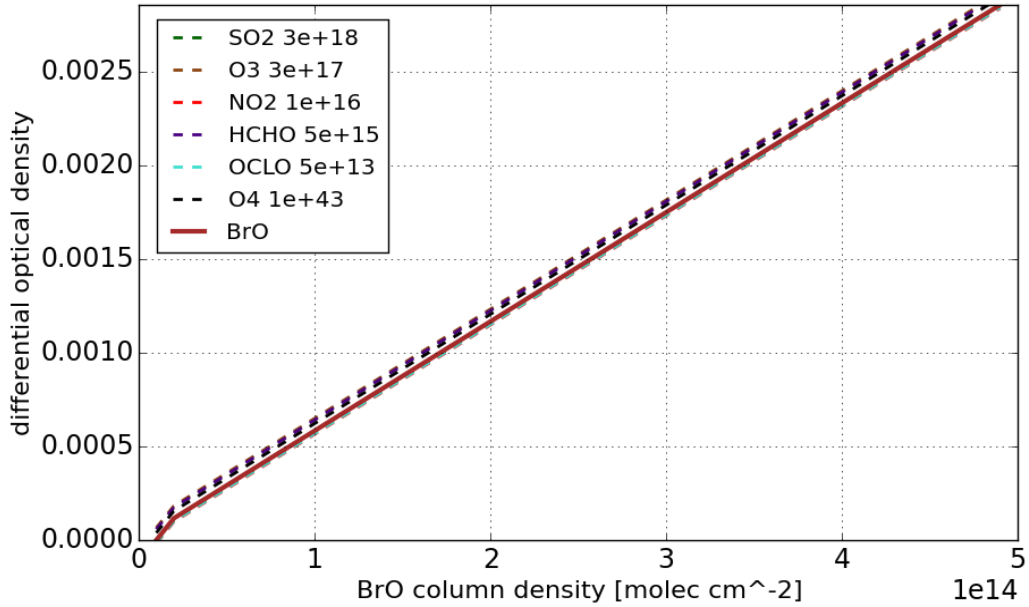

*Figure 6: simulated calibration curve of the BrO FPI measurement for typical volcanic BrO CDs. The dashed lines show the impact of typical amounts of interfering gases on the measurement, causing an uncertainty of up to ~3*10^{13} *molec* cm^{-2} *in the BrO quantification. This uncertainty can further be reduced by using more than two FPI settings.*

Photon budget of an FPI based BrO imaging device

Assuming an optical setup as described above and with specifications as shown in Table 2, we can calculate the BrO detection limits as a function of different parameters.

Table 2: Set-up parameters limiting the light throughput

Θ	a_{FPI}	η	I (see Figure 2)
1°	7.5 mm	0.25	$2*10^{11}$ ph s^{-1} mm^{-2} sr^{-1}

Table 3 shows the spatial resolution of BrO FPI imaging setups for different BrO detection limits and for an acquisition time of 1s and 5s, respectively. The absolute integrated radiances I traversing the FPI and the band pass filter were calculated with absolute radiance data from (10) and are shown in Figure 2.

Table 3: Calculated maximum pixel resolution (for arbitrary camera field of views) for different BrO detection limits and image acquisition times.

BrO det. lim. [molec cm^{-2}]	required ΔR	required $N_{ph,pix}$	pixel resolution (n_{pix} x n_{pix}) for 1s acq. time	pixel resolution (n_{pix} x n_{pix}) for 5s acq. time
$0.5*10^{14}$	$2.5*10^{-4}$	$3.2*10^{7}$	9x9 pixel	19x19 pixel
$1.0*10^{14}$	$6.0*10^{-4}$	$5.5*10^{6}$	20x20 pixel	45x45 pixel
$1.5*10^{14}$	$8.5*10^{-4}$	$2.7*10^{6}$	29x29 pixel	64x64 pixel

CONCLUSIONS

A one pixel prototype instrument was built for proving the concept of FPI based trace gas remote sensing as introduced by (8). The instrument has a high sensitivity of 1.4e-19 cm^2 $molec^{-1}$ and we did not observe cross interference to plume aerosol. This instrument can be readily extended for the detection of 2D SO_2 images with drastically reduced cross interferences compared to presently used band pass filter based SO_2 Cameras (8).

Moreover, a model study showed that the FPI technique can detect typical volcanic BrO CDs without disturbance from other gas species at high amounts as can be typically observed at volcanic sites. The photon budget allows for a detection limit of a BrO CD of 1e14 molec cm^{-2} for a 20x20 pixel resolution and an integration time of 1 second per full frame (2.5e-3 s/pix). This is by about a factor of 100 times faster than typ. dispersive DOAS measurements (18).

The FPI technique yields a high potential to visualize and quantify volcanic BrO CD distributions with high time resolution, thereby allowing the evaluation of gradients within the volcanic plume in 'real-time'. This would give unprecedented insights into short time scale halogen chemistry in volcanic plumes, which is e.g. expected to be strongly impacted by mixing with constituents of the surrounding atmosphere.

Besides volcanic studies there is a wide field of applications of the technique: It can be used to study emissions from salt lakes and even allow to study transport and chemistry events of BrO in polar regions. Moreover, the technique can be applied to many other trace gases and basically to any other process causing spectral signatures with distinct narrowband structures.

REFERENCES

1 Platt, U., & Stutz, J. (2008). Differential Optical Absorption Spectroscopy, Principles and Applications, XV, Springer, Heidelberg, 597 pp, ISBN 978-3-540-21193-8.

2 Hönninger G. and Platt U. (2002), The Role of BrO and its Vertical Distribution during Surface Ozone Depletion at Alert, Atmos. Environ., 36, 2481-2489.

3 Hönninger, G., Friedeburg, C. V., & Platt, U. (2004). Multi axis differential optical absorption spectroscopy (MAX-DOAS). Atmos. Chem. Phys., 4(1), 231-254.

4 Lohberger F., Hönninger G., and Platt U., (2004), Ground Based Imaging Differential Optical Absorption Spectroscopy of Atmospheric Gases, Appl. Opt., 43 (24), 4711-4717.

5 Platt U., Lübcke P., Kuhn J., Bobrowski N., Prata F., Burton M.R., and Kern C. (2015), Quantitative Imaging of Volcanic Plumes – Results, Future Needs, and Future Trends, J. Volcanol. Geotherm. Res., 300, 7-21.

6 Lübcke, P., Bobrowski, N., Illing, S., Kern, C., Nieves, J. A., Vogel, L., Zielcke, J., Delgado Granados, H., & Platt, U. (2013). On the absolute calibration of SO2 cameras. Atmos. Meas. Tech., 6(3), 677.

7 Dekemper, E., Vanhamel, J., Van Opstal, B., & Fussen, D. (2016). The AOTF-based NO 2 camera. Atmos. Meas. Tech., 9(12), 6025.

8 Kuhn J., Bobrowski N., Lübcke P., Vogel L., Platt U. 2014, A Fabry-Perot Interferometer Based Camera for the two-dimensional Mapping of SO_2-Distributions, Atmos. Meas. Tech. 7, 3705-3715.

9 Bobrowski, N., & Giuffrida, G. 2012. Bromine monoxide/sulphur dioxide ratios in relation to volcanological observations at Mt. Etna 2006-2009. Solid Earth, 3(2), 433.

10 Blumthaler, M., Gröbner, J., Huber, M., & Ambach, W. 1996. Measuring spectral and spatial variations of UVA and UVB sky radiance. Geophys. Res. Lett., 23(5), 547-550.

11 Fleischmann, O. C., Hartmann, M., Burrows, J. P., & Orphal, J. 2004. New ultraviolet absorption cross-sections of BrO at atmospheric temperatures measured by time-windowing Fourier transform spectroscopy. J. Photochem. Photobiol. A: Chem., 168(1), 117-132.

12 Vandaele, A. C., Hermans, C., & Fally, S. 2009. Fourier transform measurements of SO 2 absorption cross sections: II: Temperature dependence in the 29000–44000cm− 1 (227–345nm) region. J. Quant. Spectrosc. Radiat. Transfer, 110(18), 2115-2126.

13 Kromminga, H., Orphal, J., Spietz, P., Voigt, S., & Burrows, J. P. 2003. New measurements of OClO absorption cross-sections in the 325–435 nm region and their temperature dependence between 213 and 293 K. J. Photochem. Photobiol. A.: Photochem., 157(2), 149-160.

14 Bogumil, K., Orphal, J., Homann, T., Voigt, S., Spietz, P., Fleischmann, O. C., Vogel, A., Hartmann, M., Hovensmann, J., Frerick, J., & Burrows, J.P. 2003. Measurements of molecular absorption spectra with the SCIAMACHY pre-flight model: instrument characterization and reference data for atmospheric remote-sensing in the 230–2380 nm region. J. Photochem. Photobiol. A: Chem., 157(2), 167-184.

15 Chance K. and Orphal J., 2011. Revised ultraviolet absorption cross sections of H2CO for the HITRAN database. J. Quant. Spectrosc. Radiat. Trans., 112, 1509-1510.

16 Serdyuchenko, A., Gorshelev, V., Weber, M., Chehade, W., & Burrows, J. P. 2014. High spectral resolution ozone absorption cross-sections. Atmos. Meas. Tech., 7(2), 625.

17 Thalman, R., & Volkamer, R. 2013. Temperature dependent absorption cross-sections of O 2–O 2 collision pairs between 340 and 630 nm and at atmospherically relevant pressure. Phys. Chem. Chem. Phys., 15(37), 15371-15381.

18 Louban I., Bobrowski N., Rouwet D., Inguaggiato S. and Platt U. 2009. Imaging DOAS for Volcanological Applications, Bull. Volcanol. 71, 753-765.